

**Perturbative renormalization of the first moment of structure functions for domain-wall QCD**

Stefano Capitani\*

*Institut für Physik, FB Theoretische Physik, Universität Graz, A-8010 Graz, Austria*

(Received 2 November 2005; published 13 January 2006)

Using the domain-wall formulation of lattice fermions, we have computed the one-loop renormalization factors of one-link operators which measure the first nontrivial moment of the unpolarized, polarized, and transversity structure functions, in the flavor nonsinglet sector. The knowledge of these factors is necessary in order to extract physical numbers from domain-wall Monte Carlo simulations of parton distributions. We have automated the perturbative calculations by developing suitable FORM codes. The results show that in many instances the total renormalization factors are almost equal to one, and that hence the corresponding operators are, for the appropriate values of the Dirac mass  $M$  and the coupling  $g_0$ , practically unrenormalized.

DOI: [10.1103/PhysRevD.73.014505](https://doi.org/10.1103/PhysRevD.73.014505)

PACS numbers: 12.38.Gc, 11.10.Gh, 13.60.Hb

**I. INTRODUCTION**

Domain-wall fermions [1–3] provide a solution of the Ginsparg-Wilson relation [4], and as such they possess an exact chiral symmetry at nonvanishing lattice spacings [5] without at the same time presenting inconvenient features like doublers or nonanalyticities. They constitute one of the most promising formulations for simulations of chiral fermions on a lattice and for the study of physical issues connected with chirality [6]. Although Monte Carlo simulations of these fermions require more computational efforts compared with some other nonchiral formulations (like Wilson fermions), recently many advances have been reported and at present domain-wall fermions are widely used in a variety of physical situations, for which some of the most recent results and investigations can be found in [7–13].

Form factors, structure functions, and generalized parton distributions are also among the phenomenological quantities which have been studied by means of simulations with domain-wall fermions [14–17]. The calculation of the perturbative renormalization of the operators related to the moments of the deep inelastic structure functions, involving the treatment of covariant derivatives, has been missing up to now. These renormalization factors, whether perturbatively or nonperturbatively computed, are however necessary for the reliable extractions of physical numbers from Monte Carlo simulations of structure functions. The intention of the present work is to provide some of these factors from perturbation theory, and we have here considered the lowest nontrivial moment of various parton distributions. In particular, we present results for the momentum, helicity, and transversity distributions, which give a complete description of the quark momentum and spin at leading twist.

This article is organized as follows. In Sec. II we review the basic perturbative ingredients which are necessary for the calculations presented in this work, and in Sec. III we

discuss the peculiar aspects of one-loop renormalization for domain-wall fermions. In Sec. IV then we introduce the operators of which we have evaluated the renormalization factors, which we give in Sec. V. Finally, in Sec. VI we make some concluding remarks, and in the appendix we give the results for the quark self-energy and the bilinear operators, where we have found some discrepancies with old calculations [18], which however derive only from some constants in divergent continuum integrals. These discrepancies do not affect the expressions of the renormalization factors, for which there is complete agreement with Ref. [18].

**II. PERTURBATIVE DOMAIN-WALL**

We employ the standard formulation of domain-wall fermions devised by Shamir [2], where the five-dimensional quark action is given by

$$\begin{aligned}
 S_q^{\text{DW}} = & \sum_x \sum_{s=1}^{N_s} \left[ \frac{1}{2} \sum_{\mu} (\bar{\psi}_s(x)(\gamma_{\mu} - r)U_{\mu}(x)\psi_s(x + \hat{\mu}) \right. \\
 & - \bar{\psi}_s(x)(\gamma_{\mu} + r)U_{\mu}^{\dagger}(x - \hat{\mu})\psi_s(x - \hat{\mu})) \\
 & + (\bar{\psi}_s(x)P_+\psi_{s+1}(x) + \bar{\psi}_s(x)P_-\psi_{s-1}(x)) \\
 & \left. + (M - 1 + 4r)\bar{\psi}_s(x)\psi_s(x) \right] \\
 & + m \sum_x (\bar{\psi}_{N_s}(x)P_+\psi_1(x) + \bar{\psi}_1(x)P_-\psi_{N_s}(x)). \quad (1)
 \end{aligned}$$

The Wilson parameter is set to  $r = -1$ , and the Dirac mass  $M$  takes values between zero and two (at tree level) so that the correct structure of chiral modes (with no doublers) is attained for  $N_s \rightarrow \infty$ . The chiral projectors are  $P_{\pm} = (1 \pm \gamma_5)/2$ . Here and in most of the paper we put  $a = 1$ .

The above domain-wall action can be imagined as a Wilson action endowed with an additional flavor index  $s$  plus a special mass matrix for these flavors, explicitly given in Eqs. (10)–(13) further below. The mass matrix governs the mixing among the flavors and induces a sophisticated structure on the flavor space, which at the end

\*Electronic address: [stefano.capitani@uni-graz.at](mailto:stefano.capitani@uni-graz.at)

produces one light quark and  $N_s - 1$  heavy quarks. For this reason the tree-level quark propagator turns out to have a more complicated form than in the four-dimensional Wilson case, and in practical terms perturbation theory for domain-wall fermions looks like having  $N_s$  fermion flavors with an involved propagator structure in the index  $s$ . The gluon fields and their couplings to the quarks are instead kept four-dimensional, that is they do not depend on the fifth dimension and are identical at each  $s$ . The gluon propagator and vertices are then just the same as in a four-dimensional lattice theory. In this work we have used for the pure gauge part of the domain-wall action the standard plaquette action, and we perform all computations in a general covariant gauge, where the gluon propagator is given by

$$G_{\mu\nu}(k) = \frac{1}{4 \sum_{\rho} \sin^2 \frac{k_{\rho}}{2}} \left( \delta_{\mu\nu} - (1 - \alpha) \frac{4 \sin \frac{k_{\mu}}{2} \sin \frac{k_{\nu}}{2}}{4 \sum_{\lambda} \sin^2 \frac{k_{\lambda}}{2}} \right), \quad (2)$$

where  $\alpha = 1$  and  $\alpha = 0$  correspond to the Feynman and Landau gauges, respectively. The measure term, the gauge-fixing term and the Faddeev-Popov term, as well as the quark-gluon interaction vertices, have also the same expression as in the Wilson case. Since  $r = -1$ , the vertices that we need in this paper assume the form (apart from color factors)

$$V_{\mu}^{(1)}(p) = -g_0 \left( i\gamma_{\mu} \cos \frac{p_{\mu}}{2} - \sin \frac{p_{\mu}}{2} \right) \quad (3)$$

$$V_{\mu\nu}^{(2)}(p) = \frac{1}{2} g_0^2 \left( i\gamma_{\mu} \sin \frac{p_{\mu}}{2} + \cos \frac{p_{\mu}}{2} \right) \cdot \delta_{\mu\nu} \quad (4)$$

for the interaction of the quark current with one gluon and two gluons, respectively, where  $p$  stands for the sum of the incoming and outgoing quark momenta.

The construction of the tree-level quark propagator has been started in [2,19–23] and then completed and used in the first full-fledged calculations of the renormalization of the quark self-energy and bilinears [18,24,25]. Further perturbative results for domain-wall fermions have been obtained in [26–32], and some perturbative calculations for nonstandard domain-wall actions have been carried out in [33].

For our perturbative calculations with domain-wall fermions we use the same framework of [18,25], where one works solely with the dominant contributions to the propagators when the number of flavors  $N_s$  (or points in the fifth additional dimension) goes to infinity. In this limit the decoupling of the chiral modes is exact for massless quarks, chirality breaking terms being exponentially suppressed in the length of the fifth dimension.

The domain-wall Dirac operator after a Fourier transform in (four-dimensional) momentum space becomes

$$D_{st}(p) = \delta_{s,t} \sum_{\mu} i\gamma_{\mu} \sin p_{\mu} + (W_{st}^{+}(p) + mM_{st}^{+})P_{+} + (W_{st}^{-}(p) + mM_{st}^{-})P_{-}, \quad (5)$$

where the mass matrix is given by

$$W_{st}^{\pm}(p) = -W(p)\delta_{s,t} + \delta_{s\pm 1,t}, \quad (6)$$

$$M_{st}^{+} = \delta_{s,N_s} \delta_{t,1}, \quad (7)$$

$$M_{st}^{-} = \delta_{s,1} \delta_{t,N_s}, \quad (8)$$

and

$$W(p) = 1 - M + 2 \sum_{\lambda} \sin^2 \frac{p_{\lambda}}{2}. \quad (9)$$

In more explicit form,

$$W^{+}(p) = \begin{pmatrix} -W(p) & 1 & & \\ & -W(p) & \ddots & \\ & & \ddots & 1 \\ & & & -W(p) \end{pmatrix}, \quad (10)$$

$$W^{-}(p) = \begin{pmatrix} -W(p) & & & \\ 1 & -W(p) & & \\ & \ddots & \ddots & \\ & & 1 & -W(p) \end{pmatrix}, \quad (11)$$

$$M^{+} = \begin{pmatrix} & \\ 1 & \end{pmatrix}, \quad (12)$$

$$M^{-} = \begin{pmatrix} & 1 \\ & \end{pmatrix}. \quad (13)$$

We see that for  $m = 0$  the  $M^{\pm}$ 's are absent from the action and hence the propagator no longer possesses any terms directly connecting the two boundaries at  $s = 1$  and  $s = N_s$ .

In this work we only consider massless quarks. By inverting the above Dirac operator with  $m = 0$  one obtains the tree-level quark propagator

$$\begin{aligned} \langle \psi_s(-p) \bar{\psi}_t(p) \rangle &= \sum_u [(-i\gamma_{\mu} \sin p_{\mu} \delta_{s,u} \\ &+ W_{su}^{-}(p)) G_{ut}^R(p) P_{+} \\ &+ (-i\gamma_{\mu} \sin p_{\mu} \delta_{s,u} \\ &+ W_{su}^{+}(p)) G_{ut}^L(p) P_{-}]. \end{aligned} \quad (14)$$

The expressions of the functions  $G^R(p)$  and  $G^L(p)$  are, for large  $N_s$ ,

$$G_{st}^R(p) = -\frac{A(p)}{F(p)}((1 - W(p)e^{-\alpha(p)})e^{-(2N_s - s - t)\alpha(p)} + (1 - W(p)e^{\alpha(p)})e^{-(s+t)\alpha(p)} + A(p)e^{-|s-t|\alpha(p)}), \quad (15)$$

$$G_{st}^L(p) = -\frac{A(p)}{F(p)}((1 - W(p)e^{\alpha(p)})e^{-(2N_s - s - t + 2)\alpha(p)} + (1 - W(p)e^{-\alpha(p)})e^{-(s+t-2)\alpha(p)} + A(p)e^{-|s-t|\alpha(p)}), \quad (16)$$

where  $\alpha(p)$  is defined by the positive solution of the equation [2,19]

$$\cosh(\alpha(p)) = \frac{1 + W^2(p) + \sum_{\lambda} \sin^2 p_{\lambda}}{2|W(p)|}, \quad (17)$$

and

$$A(p) = \frac{1}{2W(p) \sinh(\alpha(p))}, \quad (18)$$

$$F(p) = 1 - W(p)e^{\alpha(p)}. \quad (19)$$

These formulas are only valid for positive  $W$ , which is always the case if  $0 < M < 1$ . When  $W$  has a zero,  $\alpha$  has a logarithmic singularity. For  $1 < M < 2$ ,  $W$  can become negative if the momentum is small enough. In this case the propagator is given by the above equations with the replacements

$$W \rightarrow -|W|, \quad (20)$$

$$e^{\pm\alpha} \rightarrow -e^{\pm\alpha}, \quad (21)$$

which imply that also  $\sinh\alpha$  changes sign.

To study matrix elements of the chiral modes in perturbation theory, we need to diagonalize the mass matrix in the fifth dimension. However, since this matrix is not Hermitian, one has rather to consider the squared mass matrix, that is the second-order operators  $DD^\dagger$  and  $D^\dagger D$ , which are Hermitian and nonnegative and give a well-behaved spectrum. In the second-order operators the two chiralities are in fact well decoupled.

The chiral mode is obtained by means of a rotation in the fifth dimension of the original quark fields  $\psi_s(x)$  to the basis which diagonalizes the mass matrix, and is given by

$$\chi_0(x) = \sqrt{1 - w_0^2} \sum_s (P_+ w_0^{s-1} \psi_s(x) + P_- w_0^{N_s - s} \psi_s(x)), \quad (22)$$

where

$$w_0 = W(0) = 1 - M. \quad (23)$$

We can see that, because of the damping factors  $w_0^{s-1}$  and  $w_0^{N_s - s}$ , the chiral mode is exponentially localized near the

boundaries of the fifth dimension. The ‘‘physical’’ quark fields that are instead used in Monte Carlo simulations are however somewhat simpler, and they are constructed only from quark fields exactly located at these boundaries:

$$q(x) = P_+ \psi_1(x) + P_- \psi_{N_s}(x) \quad (24)$$

$$\bar{q}(x) = \bar{\psi}_{N_s}(x) P_+ + \bar{\psi}_1(x) P_-. \quad (25)$$

We also use these expressions for our calculations, as done in [18,24,25].

The computation of matrix elements involving states and operators constructed from these physical quark fields requires additional propagators. We need in fact to connect an internal with a physical quark field, and the corresponding propagators are given by

$$\begin{aligned} \langle q(-p) \bar{\psi}_s(p) \rangle &= \frac{1}{F(p)} i\gamma_{\mu} \sin p_{\mu} (e^{-(N_s - s)\alpha(p)} P_+ \\ &+ e^{-(s-1)\alpha(p)} P_-) \\ &- e^{-\alpha(p)} (e^{-(s-1)\alpha(p)} P_+ \\ &+ e^{-(N_s - s)\alpha(p)} P_-), \end{aligned} \quad (26)$$

$$\begin{aligned} \langle \psi_s(-p) \bar{q}(p) \rangle &= \frac{1}{F(p)} (e^{-(N_s - s)\alpha(p)} P_- \\ &+ e^{-(s-1)\alpha(p)} P_+) i\gamma_{\mu} \sin p_{\mu} \\ &- e^{-\alpha(p)} (e^{-(s-1)\alpha(p)} P_- \\ &+ e^{-(N_s - s)\alpha(p)} P_+). \end{aligned} \quad (27)$$

For our calculations it is also necessary to know their expansions for small momentum:

$$\begin{aligned} \langle q(-p) \bar{\psi}_s(p) \rangle_c &= \frac{1 - w_0^2}{i\not{p}} \left( w_0^{N_s - s} P_+ + w_0^{s-1} P_- \right. \\ &\left. - \frac{w_0}{1 - w_0^2} i\not{p} (w_0^{s-1} P_+ + w_0^{N_s - s} P_-) \right), \end{aligned} \quad (28)$$

$$\begin{aligned} \langle \psi_s(-p) \bar{q}(p) \rangle_c &= \left( w_0^{N_s - s} P_- + w_0^{s-1} P_+ \right. \\ &\left. - (w_0^{s-1} P_- + w_0^{N_s - s} P_+) \frac{w_0}{1 - w_0^2} i\not{p} \right) \\ &\times \frac{1 - w_0^2}{i\not{p}}, \end{aligned} \quad (29)$$

where the factors  $1 - w_0^2$  are related to the sums of the tree-level exponential damping factors over the fifth dimension:

$$\lim_{N_s \rightarrow \infty} \sum_{s=1}^{N_s} (w_0^{N_s - s} P_+ + w_0^{s-1} P_-)^2 = \frac{1}{1 - w_0^2}. \quad (30)$$

Finally, we also need the tree-level propagator

$$\langle q(-p)\bar{q}(p) \rangle = \frac{i\gamma_\mu \sin p_\mu}{F(p)}, \quad (31)$$

which in the limit of small momentum is equal to

$$\langle q(-p)\bar{q}(p) \rangle_c = \frac{1 - w_0^2}{i\not{p}}. \quad (32)$$

### III. ONE-LOOP RENORMALIZATION

Matrix elements estimated by importance sampling in Monte Carlo lattice simulations need to be properly renormalized in order to become meaningful physical numbers. They can be considered as (regulated) bare quantities, and in order to get physical results they have to undergo a lattice renormalization which matches them to some continuum scheme. We choose for the continuum the  $\overline{\text{MS}}$  scheme of dimensional regularization, since commonly Wilson coefficients of operator product expansions are computed in this scheme.

A perturbative lattice renormalization involves both lattice and continuum perturbative calculations. At tree level, for momenta much lower than the lattice cutoff, lattice operators have the same matrix elements as the original continuum operators. At one loop one then gets, for the case of a multiplicatively renormalized operator,

$$\langle q|O^{\text{lat}}|q \rangle = (1 + \bar{g}^2(-\gamma^{(0)} \log a^2 p^2 + R^{\text{lat}})) \cdot \langle q|O^{\text{tree}}|q \rangle, \quad (33)$$

$$\langle q|O^{\overline{\text{MS}}}|q \rangle = \left(1 + \bar{g}_{\overline{\text{MS}}}^2 \left(-\gamma^{(0)} \log \frac{p^2}{\mu^2} + R^{\overline{\text{MS}}}\right)\right) \cdot \langle q|O^{\text{tree}}|q \rangle, \quad (34)$$

where the lattice and continuum one-loop finite constants,  $R^{\text{lat}}$  and  $R^{\overline{\text{MS}}}$ , do not have in general the same value, and hence the one-loop renormalization factors on the lattice and in the continuum are in general not equal (the one-loop anomalous dimensions are however the same). Here and in the following we call for brevity  $\bar{g}^2 = (g_0^2/16\pi^2)C_F$  (and similarly for  $\bar{g}_{\overline{\text{MS}}}^2$ ), with  $C_F = (N_c^2 - 1)/2N_c$  for the  $\text{SU}(N_c)$  gauge group.

The connection between the original lattice numbers and the final continuum physical results is given, neglecting higher-order terms in  $\bar{g}^2$ , by [34]

$$\frac{\langle q|O^{\overline{\text{MS}}}|q \rangle}{\langle q|O^{\text{lat}}|q \rangle} = 1 - \bar{g}^2(-\gamma^{(0)} \log a^2 \mu^2 + R^{\text{lat}} - R^{\overline{\text{MS}}}), \quad (35)$$

where the difference  $\Delta R = R^{\text{lat}} - R^{\overline{\text{MS}}}$  determines the renormalization factor

$$Z_O(a\mu, \bar{g}) = 1 - \bar{g}^2(-\gamma^{(0)} \log a^2 \mu^2 + \Delta R) \quad (36)$$

which converts the lattice operator  $O^{\text{lat}}$  into the physical

renormalized operator  $O^{\overline{\text{MS}}}$ . The computation of these renormalization factors requires both lattice and continuum perturbative techniques (for more details see [35]). In the domain-wall case it presents additional peculiar features that is worth reviewing.

Let us first consider, in the massless case, the one-loop correction to the domain-wall quark propagator  $\langle q(-p)\bar{q}(p) \rangle_c$ . It can be easily seen that, given the structure of the propagators  $\langle q(-p)\bar{\psi}_s(p) \rangle_c$  and  $\langle \psi_s(-p)\bar{q}(p) \rangle_c$ , we can write

$$\langle q(-p)\bar{q}(p) \rangle_{\text{1loop}} = \frac{1 - w_0^2}{i\not{p}} \Sigma_q(p) \frac{1 - w_0^2}{i\not{p}} \quad (37)$$

$$= \frac{1 - w_0^2}{i\not{p} - (1 - w_0^2)\Sigma_q(p)}, \quad (38)$$

where

$$\begin{aligned} \Sigma_q(p) = & \sum_{s,t} \left( w_0^{N_s - s} P_+ + w_0^{s-1} P_- \right. \\ & \left. - \frac{w_0}{1 - w_0^2} i\not{p} (w_0^{s-1} P_+ + w_0^{N_s - s} P_-) \right) \\ & \cdot \Sigma_{st}(p) \cdot \left( w_0^{N_s - t} P_- + w_0^{t-1} P_+ \right. \\ & \left. - (w_0^{t-1} P_- + w_0^{N_s - t} P_+) \frac{w_0}{1 - w_0^2} i\not{p} \right). \end{aligned} \quad (39)$$

The calculation of the one-loop self-energy diagrams gives [18]

$$\Sigma_{st}(p) = -\bar{g}^2(i\not{p}(I^+ P_+ + I^- P_-) + W_1^+ P_+ + W_1^- P_-)_{st}, \quad (40)$$

and when the damping factors are also taken into account the final result can be written as

$$\Sigma_q(p) = \frac{1}{1 - w_0^2} i\not{p} \bar{g}^2 \left( \alpha \log a^2 p^2 + \Sigma_1 - \frac{2w_0}{1 - w_0^2} \Sigma_3 \right). \quad (41)$$

Putting all together, we see that the one-loop correction to the quark propagator is of the same form as its tree-level expression:

$$\langle q(-p)\bar{q}(p) \rangle_{\text{1loop}} = \frac{1 - w_0^2}{i\not{p} - (1 - w_0^2)\Sigma_q(p)} = \frac{1 - w_0^2}{i\not{p}} Z_w Z_2, \quad (42)$$

where

$$Z_2 = 1 + \bar{g}^2(\alpha \log a^2 p^2 + \Sigma_1) \quad (43)$$

is the usual quark wave function renormalization factor, whereas

$$Z_w = 1 - \frac{2w_0}{1 - w_0^2} \bar{g}^2 \Sigma_3 = 1 + \bar{g}^2 z_w \quad (44)$$

is a new feature appearing in domain-wall fermions, which represents an additive renormalization to  $w_0$ , as can be seen from

$$(1 - w_0^2)Z_w = 1 - (w_0 + \bar{g}^2 \Sigma_3)^2 + O(\bar{g}^4). \quad (45)$$

Thus, while the zero mode remains stable under radiative corrections, the Dirac mass  $M = 1 - w_0$  is additively renormalized. This effect is due to the  $W_1^\pm$  terms in Eq. (40), which in turn originate from the order  $a$  terms in the damping factors of Eqs. (28) and (29). We have by explicit calculation checked that the part proportional to  $1 - \alpha$  of  $\Sigma_3$  is zero (its contribution from the half-circle diagram exactly canceling the one of the tadpole), which means that  $\Sigma_3$  and  $Z_w$  are gauge invariant. The values of  $\Sigma_1$ ,  $\Sigma_3$ , and  $z_w$  can be found in the appendix.

We remark that in the above domain-wall self-energy there is no term  $\Sigma_0$  proportional to  $1/a$ , which if present would signal a breaking of chirality.

Let us now consider a composite operator  $\bar{q}(x)Oq(x)$  which is multiplicatively renormalizable. Again, by looking at the form of the propagators involved, one can see

that the one-loop matrix element of this operator between physical quark states is given by

$$\langle (\bar{q}Oq)q\bar{q} \rangle_{\text{1loop}} = \frac{1 - w_0^2}{i\not{p}} \cdot A_O(p) \cdot O \cdot \frac{1 - w_0^2}{i\not{p}}, \quad (46)$$

where  $A_O(p)$  contains the contribution of the damping factors and can be written as

$$A_O(p) = \bar{g}^2(-\gamma_0 \log a^2 p^2 + B_O). \quad (47)$$

The one-loop expression has the same form as the tree-level matrix element. That also the self-energy contribution to the matrix element fits properly here can be seen (for example when  $O = \gamma_\mu$ ) from inserting Eq. (41) (without  $\Sigma_3$ ) in the expression of the contribution of a leg in Fig. 1,

$$\begin{aligned} & \frac{1 - w_0^2}{i\not{p}} \cdot \frac{1}{1 - w_0^2} i\not{p} \cdot \bar{g}^2(\alpha \log a^2 p^2 + \Sigma_1) \\ & \cdot \frac{1 - w_0^2}{i\not{p}} \gamma_\mu \frac{1 - w_0^2}{i\not{p}}, \end{aligned} \quad (48)$$

which shows that indeed it gives a multiplicative correction to the tree-level matrix element:

$$\frac{1 - w_0^2}{i\not{p}} \cdot \bar{g}^2(\alpha \log a^2 p^2 + \Sigma_1) \cdot \gamma_\mu \cdot \frac{1 - w_0^2}{i\not{p}}. \quad (49)$$

#### IV. STRUCTURE FUNCTION OPERATORS

The operators that we have considered in this work measure the lowest moment of various structure functions. They include all three parton distributions that characterize the quarks in the nucleon: the momentum distribution  $q(x, Q^2)$  (described by the  $F_1$  and  $F_2$  unpolarized structure functions), the helicity distribution  $\Delta q(x, Q^2)$  (described by the  $g_1$  structure function), and the (chiral-odd) transversity distribution  $\delta q(x, Q^2)$  (described by the  $h_1$  structure function). They thus provide a complete description of quark momentum and spin at leading twist. We have also computed the renormalization of the lowest moment of the  $g_2$  structure function, which receives contributions from twist-3 operators and measures the (chiral-even) transverse spin. We refer for a more detailed discussion of these structure functions and, in particular, of the operators appearing in their operator product expansions, some of which are given below, to [36,37] (of which we follow the notation) and references therein.

We have computed the renormalization factors of all flavor nonsinglet operators which contain at most one covariant derivative. We have chosen in particular

$$O_{v_2,d} = \bar{q} \gamma_{\{1} D_4 q, \quad (50)$$

$$O_{v_2,e} = \bar{q} \gamma_4 D_4 q - \frac{1}{3} \sum_{i=1}^3 \bar{q} \gamma_i D_i q, \quad (51)$$

which measure the first moment of the momentum distri-

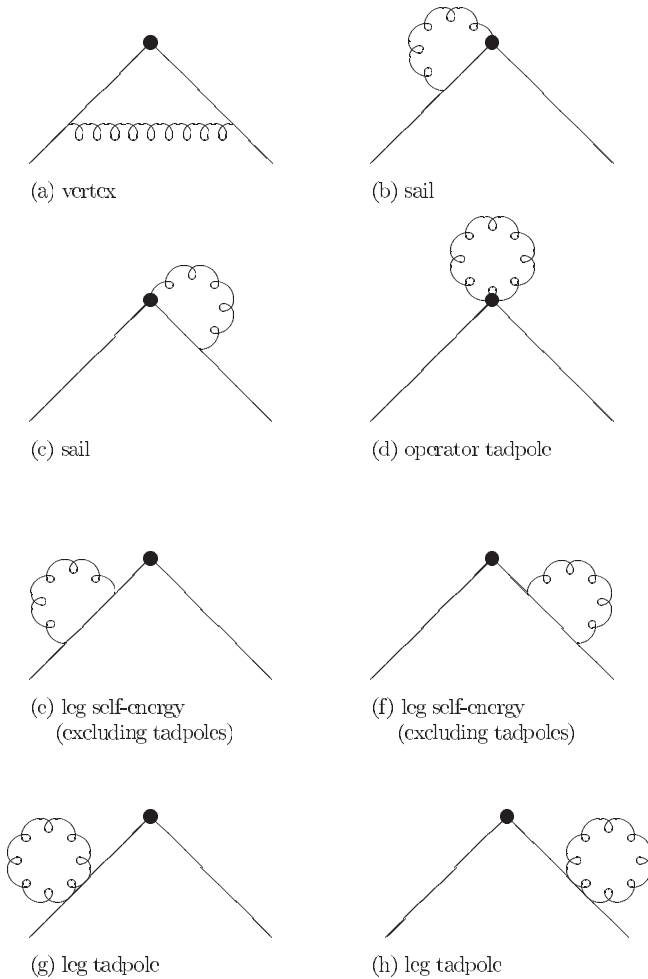


FIG. 1. The diagrams needed for the one-loop renormalization of the lattice operators.

butions,

$$O_{a_2,d} = \bar{q}\gamma_{\{1}\gamma_5 D_{4\}}q, \quad (52)$$

$$O_{a_2,e} = \bar{q}\gamma_4\gamma_5 D_4 q - \frac{1}{3} \sum_{i=1}^3 \bar{q}\gamma_i\gamma_5 D_i q, \quad (53)$$

which measure the first moment of the helicity distributions,

$$O_{d_1} = \bar{q}\gamma_{[4}\gamma_5 D_{1]}q, \quad (54)$$

which taken together with  $O_{a_2}$  determines the first moment of the  $g_2$  structure function, and finally

$$O_{t_1} = \bar{q}\sigma_{41}\gamma_5 q, \quad (55)$$

$$O_{t_2} = \bar{q}\sigma_{4\{1}\gamma_5 D_{2\}}q, \quad (56)$$

which correspond to the tensor charge and the lowest nontrivial moment of the  $h_1$  transversity structure function, respectively. We have not explicitly shown the Gell-Mann flavor matrices which specialize them to nonsinglet operators and hence forbid any mixing with gluonic operators, because they are irrelevant for the sake of the calculation of the renormalization factors. The symbol  $\{\}$  denotes symmetrization over the relevant Lorentz indices, while  $[\ ]$  denotes antisymmetrization. For the covariant derivatives  $D = \vec{D} - \overleftarrow{D}$  we use the lattice discretizations

$$\vec{D}_\mu q(x) = \frac{1}{2}[U_\mu(x)q(x + \hat{\mu}) - U_\mu^\dagger(x - \hat{\mu})q(x - \hat{\mu})] \quad (57)$$

$$\overleftarrow{D}_\mu q(x) = \frac{1}{2}[\bar{q}(x + \hat{\mu})U_\mu^\dagger(x) - \bar{q}(x - \hat{\mu})U_\mu(x - \hat{\mu})]. \quad (58)$$

We have in some cases considered two representatives for an operator measuring a given parton distribution. They are differentiated and identified by the choice of their Lorentz indices. The lattice operators corresponding to these choices fall in two different irreducible representations of the hypercubic group (the symmetry group of the lattice, the remnant of the Lorentz symmetry), and on the lattice they will renormalize in a different way (whereas in a continuum scheme their renormalization factors are equal). In Monte Carlo measurements one of the two choices can be more convenient to use than the other, giving for instance smaller statistical and systematic errors, in particular, when one considers the role played by non-vanishing momenta in numerical simulations.

Since we have done the calculations with  $N_s = \infty$ , an exact chiral symmetry is maintained in all our results, and its most important consequence is that the operator which measures the lowest moment of the  $g_2$  structure function does not show any of the power-divergent mixings with operators of lower dimension which are instead present in

the case of Wilson fermions. In fact, when chiral symmetry is broken  $O_{d_1}$  mixes with a lower-dimensional operator which in the continuum operator product expansion is

$$m_q \bar{q}\gamma_{[4}\gamma_5\gamma_{1]}q, \quad (59)$$

but on the lattice instead has, in place of the mass, a  $1/a$  coefficient which becomes infinite in the continuum limit. This mixing is forbidden for domain-wall fermions with infinite  $N_s$ , and  $O_{d_1}$  is then in this case multiplicatively renormalized. In addition, chiral symmetry implies that the renormalization constants of corresponding unpolarized and polarized operators (which differ by a  $\gamma_5$  matrix) assume the same value. Thus, chiral symmetry gives a reduction of the number of independent renormalization factors in a given physical situation.

For operators which contain one covariant derivative one needs to perform a Taylor expansion of all vertices and propagators at first order in the lattice spacing  $a$  (which means the external momentum  $p$ ). We have chosen as loop integration momentum the one carried by the internal quarks. Choosing the one carried by the gluon would result in much more complicated expressions for the order  $p$  contributions.

## V. RESULTS

The diagrams required for the one-loop lattice calculations of the matrix elements that we have considered here are given in Fig. 1. It can be easily seen that all tadpole diagrams are diagonal in the fifth dimension, and therefore they are equal to the expression calculated with Wilson fermions. A leg tadpole has then the value

$$T_l = 8\pi^2 Z_0 (1 - \frac{1}{4}(1 - \alpha)), \quad (60)$$

where  $Z_0 = 0.154933390231\dots$  is a well-known integral [35], while the operator tadpoles have the expression

$$T_O = -T_l \quad (61)$$

for all operators considered in this work except the tensor charge, for which the operator tadpole vanishes,  $T_{t_1} = 0$  [36,37]. The half-circle contribution of the quark self-energy as well as the vertex and sail diagrams instead all have a nontrivial structure in the fifth dimension, and due to their complexity we have deemed necessary to compute them using computer programs.

We have used the algebraic manipulation program FORM [38] to construct routines able to carry out all needed analytic calculations in an automated way. Sums of the damping factors in the fifth dimension and of the four-dimensional expressions in momentum space are evaluated with Fortran programs. To improve the convergence of the numerical integrals we use some of the techniques given by Lüscher and Weisz in [39].

The one-loop diagrams of Fig. 1 diverge at most logarithmically. Special care is required for the evaluation of

the divergent terms, for which it is convenient to use the method introduced by Kawai *et al.* in [40] (see also [35] for simple examples). A logarithmically divergent integral

$$I(p) = \int dk I(k, p) \quad (62)$$

is expanded in powers of the external momentum and split as

$$I(p) = J(0) + (I(p) - J(0)), \quad (63)$$

where

$$J(0) = \int dk I(k, 0) \quad (64)$$

is its Taylor expansion to lowest order in  $p$ . Since the integrals appearing in  $J$  do not depend on the external momentum, they are much easier to compute on the lattice than the complete integral of type  $I$ . The whole dependence on the external momentum remains in  $I - J$ , which is ultraviolet-finite for  $a \rightarrow 0$  and can be evaluated by taking the naive continuum limit. Thanks to these facts, one is left with computing on the lattice only integrals with vanishing momentum, which is technically straightforward. It is to be remarked that while  $I$  is well defined, for finite lattice spacing both  $J$  and  $I - J$  are separately infrared divergent. To compute them one must then introduce an intermediate regularization, which we choose to be the naive dimensional regularization. The associated divergences will at the end cancel out in the sum  $J + (I - J)$ .

To summarize, using this method the computation of any divergent integral which depends on an external momentum is reduced to the computation of lattice integrals at zero momentum plus some continuum integrals.

Identifying and processing divergent terms in an automated way for domain-wall fermions turns out to be somewhat more complicated and prone to errors than for simpler cases like Wilson fermions. We have thus devised an alternative indirect procedure for the evaluation of divergent integrals. This procedure uses the chain of equalities

$$I^{\text{DW}} = J^{\text{DW}} + (I^{\text{DW}} - J^{\text{DW}}) \quad (65)$$

$$= J^{\text{DW}} + (I^{\text{W}} - J^{\text{W}}) = (J^{\text{DW}} - J^{\text{W}}) + I^{\text{W}}, \quad (66)$$

where DW stands for domain-wall and W for Wilson fermions. In words, we numerically compute the difference between the domain-wall and Wilson zero-momentum  $J$  integrals, and then add the full well-known Wilson result (for which several significant digits can be obtained without much effort). The key points here are that the difference  $J^{\text{DW}} - J^{\text{W}}$  is a finite lattice integral, because the above-mentioned infrared divergences exactly cancel, and thus it does not need to be regularized at all, and moreover that the difference  $I - J$  is an integral taken in the continuum limit, and so it makes no difference whether it is evaluated using domain-wall or Wilson fermions.

We have tested that our procedure works as desired by applying it to calculations with overlap fermions, and we have reproduced in this way all results known in the literature for the bilinear operators [41] and the first moment of the unpolarized parton distribution [36,37]. This procedure is also much more precise than the subtraction of a known simple lattice integral with the same divergent behavior, which has the disadvantage of sometimes converging very slowly and hence it requires very large integration grids to attain the same accuracy. In a few cases we have used the simpler method (which gives just a couple of significant digits) for consistency checks.

The amputated matrix elements that we have calculated have on the lattice the form (see Eq. (47))

$$1 + \bar{g}^2(-\gamma_O \log a^2 p^2 + B_O), \quad (67)$$

with

$$B_O = V_O + T_O + \Sigma_1, \quad (68)$$

where  $V_O$  is the finite contribution of the vertex and sail diagrams (Fig. 1(a)–1(c)),  $T_O$  refers to the tadpole arising from the operator (Fig. 1(d)), and  $\Sigma_1$  is the finite contribution (proportional to  $i\not{p}$ ) from the quark self-energy of one leg, which also includes a leg tadpole (Fig. 1(e) and 1(g) or Fig. 1(f) and 1(h)). We call “proper” contributions the ones that do not include the self-energy. They correspond to the diagrams a-d in Fig. 1. Calling  $1 - \alpha = \xi$ , the one-loop results for them are:

$$O_{v_2,d}^{\text{proper}} = \bar{g}^2\left(\frac{\xi}{3} + \xi\right) \log a^2 p^2 + V_{v_2,d}^{\alpha=1} - \xi \cdot 6.850\,272 + T_{v_2,d} O_{v_2,d}^{\text{tree}}, \quad (69)$$

$$O_{a_2,d}^{\text{proper}} = \bar{g}^2\left(\frac{\xi}{3} + \xi\right) \log a^2 p^2 + V_{a_2,d}^{\alpha=1} - \xi \cdot 6.850\,272 + T_{a_2,d} O_{a_2,d}^{\text{tree}}, \quad (70)$$

$$O_{v_2,e}^{\text{proper}} = \bar{g}^2\left(\frac{\xi}{3} + \xi\right) \log a^2 p^2 + V_{v_2,e}^{\alpha=1} - \xi \cdot 6.850\,272 + T_{v_2,e} O_{v_2,e}^{\text{tree}}, \quad (71)$$

$$O_{a_2,e}^{\text{proper}} = \bar{g}^2\left(\frac{\xi}{3} + \xi\right) \log a^2 p^2 + V_{a_2,e}^{\alpha=1} - \xi \cdot 6.850\,272 + T_{a_2,e} O_{a_2,e}^{\text{tree}}, \quad (72)$$

$$O_{d_1}^{\text{proper}} = \bar{g}^2((-1 + \xi) \log a^2 p^2 + V_{d_1}^{\alpha=1} - \xi \cdot 7.850\,272 + T_{d_1}) O_{d_1}^{\text{tree}}, \quad (73)$$

$$O_{t_1}^{\text{proper}} = \bar{g}^2(\xi \log a^2 p^2 + V_{t_1}^{\alpha=1} - \xi \cdot 3.792\,010) O_{t_1}^{\text{tree}}, \quad (74)$$

$$O_{t_2}^{\text{proper}} = \bar{g}^2((2 + \xi) \log a^2 p^2 + V_{t_2}^{\alpha=1} - \xi \cdot 6.350\,272 + T_{t_2}) O_{t_2}^{\text{tree}}. \quad (75)$$

The results due to the sails and vertices,  $V_O$ , have been for

convenience separated in the Feynman gauge values  $V_0^{\alpha=1}$ , listed in Table I for various choices of the Dirac mass  $M$  between  $M = 0.1$  and  $M = 1.9$ , and the remaining contributions proportional to  $\xi$ , which are instead independent of  $M$  and shown in the above equations. Notice that also the tadpoles coming from the operators provide contributions proportional to  $\xi$ . The results for the tensor charge,  $V_{t_1}$ , are equal to the results for the standard tensor current  $\bar{q}\sigma_{\mu\nu}q$ , which were already calculated in [18], and are reported, together with the other bilinears and the self-energy results, in the appendix.

A significant check of our perturbative calculations is that the contributions proportional to  $\xi$  in covariant gauge are constant in  $M$ , as already noted in [35–37] for the case of overlap fermions and discussed more in depth in [42]. Furthermore, they are equal to the results obtained with Wilson fermions (and this is the reason why we can provide more significant digits for these contributions). They are also independent of the lattice representation of the operator (e.g., for  $O_{v_2,d}$  and  $O_{v_2,e}$ ). Their analytic expressions are very complicated and highly nonlinear functions of  $M$  containing hundreds of terms, and the numerical cancellation of this dependence is a rather strong check on the good behavior of the FORM codes, as well as of the integration routines.

TABLE I. Values for the sums of the vertex and sail diagrams,  $V_0^{\alpha=1}$ , for the momentum, helicity, and transversity operators considered in this work, in Feynman gauge. The one-loop results of the proper diagrams in a general covariant gauge can be inferred from Eqs. (69)–(75). We remind that  $V_{a_2,d}^{\alpha=1} = V_{v_2,d}^{\alpha=1}$  and  $V_{a_2,e}^{\alpha=1} = V_{v_2,e}^{\alpha=1}$ . The case of the tensor charge,  $V_{t_1}^{\alpha=1}$ , has been calculated for the first time in [18].

$M$	$V_{v_2,d}^{\alpha=1}$	$V_{v_2,e}^{\alpha=1}$	$V_{d_1}^{\alpha=1}$	$V_{t_1}^{\alpha=1}$	$V_{t_2}^{\alpha=1}$
0.1	-3.6205	-3.2261	96.1427	5.1733	-3.8636
0.2	-3.5296	-3.1111	42.4140	4.9150	-3.8433
0.3	-3.4553	-3.0116	25.0326	4.7069	-3.8223
0.4	-3.3896	-2.9194	16.5587	4.5245	-3.8004
0.5	-3.3288	-2.8310	11.5737	4.3571	-3.7776
0.6	-3.2711	-2.7441	8.2910	4.1987	-3.7539
0.7	-3.2150	-2.6573	5.9508	4.0454	-3.7291
0.8	-3.1597	-2.5694	4.1741	3.8943	-3.7031
0.9	-3.1042	-2.4795	2.7486	3.7427	-3.6758
1.0	-3.0478	-2.3865	1.5425	3.5882	-3.6472
1.1	-2.9898	-2.2894	0.4655	3.4286	-3.6170
1.2	-2.9293	-2.1869	-0.5533	3.2610	-3.5850
1.3	-2.8652	-2.0776	-1.5787	3.0821	-3.5510
1.4	-2.7964	-1.9598	-2.6834	2.8879	-3.5148
1.5	-2.7209	-1.8311	-3.9675	2.6727	-3.4760
1.6	-2.6362	-1.6880	-5.5992	2.4284	-3.4342
1.7	-2.5384	-1.5258	-7.9262	2.1425	-3.3889
1.8	-2.4203	-1.3360	-11.8927	1.7930	-3.3395
1.9	-2.2671	-1.1022	-21.7691	1.3341	-3.2850

Another reasonably strong check is that the operators  $O_{v_2,d}$  and  $O_{a_2,d}$  have the same renormalization constant well within the numerical integration errors, as expected from chiral symmetry. We have checked that this is also true for the pair  $O_{v_2,e}$  and  $O_{a_2,e}$ . Thus, in all cases the polarized operators have the same renormalization constants as the corresponding unpolarized operators. Furthermore, as we have explicitly verified, for the same reason the  $1/a$  coefficient of the mixing term of Eq. (59) arising in the one-loop expression of the operator  $O_{d_1}$  tends to zero when the integration grid is refined. This operator is then for domain-wall fermions multiplicatively renormalized, contrary to what happens in the Wilson case, where its mixing coefficient goes to infinity in the continuum limit.

In the numerical integration, the convergence can become slow when  $M$  is very close to zero or two. Thus, while otherwise a grid of 60 or 80 points in each direction is sufficient to obtain about five significant digits, for  $M = 0.1$  and  $M = 1.9$  we had sometimes to increase the grid to 100 points in each direction in order to achieve the same precision.

To obtain the complete one-loop amplitudes we have now to add to the results of the proper diagrams the 1-loop contributions of the self-energy which are proportional to  $i\not{p}$ ,

$$\Sigma_1 = \bar{g}^2((1 - \xi) \log a^2 p^2 + \Sigma_1^{\alpha=1} + \xi \cdot 4.792010), \quad (76)$$

where  $\Sigma_1^{\alpha=1} = 10.8750$  when  $M = 1$ , while for other values of  $M$  the Feynman-gauge finite terms  $\Sigma_1^{\alpha=1}$  are given in the appendix. The complete one-loop lattice results are then, for  $M = 1$ :

$$O_{v_2,d}^{\text{lat}} = (1 + \bar{g}^2(\frac{8}{3} \log a^2 p^2 - 4.4059 + \xi)) O_{v_2,d}^{\text{tree}}, \quad (77)$$

$$O_{a_2,d}^{\text{lat}} = (1 + \bar{g}^2(\frac{8}{3} \log a^2 p^2 - 4.4059 + \xi)) O_{a_2,d}^{\text{tree}}, \quad (78)$$

$$O_{v_2,e}^{\text{lat}} = (1 + \bar{g}^2(\frac{8}{3} \log a^2 p^2 - 3.7445 + \xi)) O_{v_2,e}^{\text{tree}}, \quad (79)$$

$$O_{a_2,e}^{\text{lat}} = (1 + \bar{g}^2(\frac{8}{3} \log a^2 p^2 - 3.7445 + \xi)) O_{a_2,e}^{\text{tree}}, \quad (80)$$

$$O_{d_1}^{\text{lat}} = (1 + \bar{g}^2 \cdot 0.1845) O_{d_1}^{\text{tree}}, \quad (81)$$

$$O_{t_1}^{\text{lat}} = (1 + \bar{g}^2(\log a^2 p^2 + 14.4633 + \xi)) O_{t_1}^{\text{tree}}, \quad (82)$$

$$O_{t_2}^{\text{lat}} = (1 + \bar{g}^2(3 \log a^2 p^2 - 5.0052 + \frac{3}{2}\xi)) O_{t_2}^{\text{tree}}. \quad (83)$$

To establish the connection with the corresponding continuum quantities we also need to know the one-loop amplitudes for the same operators in the  $\overline{\text{MS}}$  scheme [36,37]:

$$O_{v_2}^{\overline{\text{MS}}} = \left(1 + \bar{g}^2 \left( \frac{8}{3} \log \frac{p^2}{\mu^2} - \frac{40}{9} + \xi \right)\right) O_{v_2}^{\text{tree}}, \quad (84)$$

$$O_{a_2}^{\overline{\text{MS}}} = \left(1 + \bar{g}^2 \left( \frac{8}{3} \log \frac{p^2}{\mu^2} - \frac{40}{9} + \xi \right)\right) O_{a_2}^{\text{tree}}, \quad (85)$$

$$O_{d_1}^{\overline{\text{MS}}} = O_{d_1}^{\text{tree}}, \quad (86)$$

$$O_{t_1}^{\overline{\text{MS}}} = \left(1 + \bar{g}^2 \left( \log \frac{p^2}{\mu^2} - 1 + \xi \right)\right) O_{t_1}^{\text{tree}}, \quad (87)$$

$$O_{t_2}^{\overline{\text{MS}}} = \left(1 + \bar{g}^2 \left( 3 \log \frac{p^2}{\mu^2} - 5 + \frac{3}{2} \xi \right)\right) O_{t_2}^{\text{tree}}. \quad (88)$$

Putting all together, we obtain the factors that allow the matching from the domain-wall lattice theory to the  $\overline{\text{MS}}$  continuum scheme, for  $M = 1$ :

$$O_{v_2,d}^{\overline{\text{MS}}} = (1 - \bar{g}^2 (\frac{8}{3} \log a^2 \mu^2 + 0.0386)) O_{v_2,d}^{\text{lat}}, \quad (89)$$

$$O_{a_2,d}^{\overline{\text{MS}}} = (1 - \bar{g}^2 (\frac{8}{3} \log a^2 \mu^2 + 0.0386)) O_{a_2,d}^{\text{lat}}, \quad (90)$$

$$O_{v_2,e}^{\overline{\text{MS}}} = (1 - \bar{g}^2 (\frac{8}{3} \log a^2 \mu^2 + 0.6999)) O_{v_2,e}^{\text{lat}}, \quad (91)$$

$$O_{a_2,e}^{\overline{\text{MS}}} = (1 - \bar{g}^2 (\frac{8}{3} \log a^2 \mu^2 + 0.6999)) O_{a_2,e}^{\text{lat}}, \quad (92)$$

$$O_{d_1}^{\overline{\text{MS}}} = (1 + \bar{g}^2 \cdot 0.1845) O_{d_1}^{\text{lat}}, \quad (93)$$

$$O_{t_1}^{\overline{\text{MS}}} = (1 - \bar{g}^2 (\log a^2 \mu^2 + 15.4633)) O_{t_1}^{\text{lat}}, \quad (94)$$

$$O_{t_2}^{\overline{\text{MS}}} = (1 - \bar{g}^2 (3 \log a^2 \mu^2 - 0.0052)) O_{t_2}^{\text{lat}}. \quad (95)$$

Notice that the part proportional to  $\xi$  has canceled between the lattice and continuum expressions, and these renormalization factors are hence gauge invariant.

For simulations of domain-wall QCD at  $g_0 = 1$ , setting  $\mu = 1/a$  one obtains the values

$$\begin{aligned} O_{v_2,d}^{\overline{\text{MS}}} &= 0.9997 \cdot O_{v_2,d}^{\text{lat}(\text{domain-wall}, M=1.0)} \\ &= 0.98920 \cdot O_{v_2,d}^{\text{lat}(\text{Wilson})}, \end{aligned} \quad (96)$$

$$\begin{aligned} O_{a_2,d}^{\overline{\text{MS}}} &= 0.9997 \cdot O_{a_2,d}^{\text{lat}(\text{domain-wall}, M=1.0)} \\ &= 0.99709 \cdot O_{a_2,d}^{\text{lat}(\text{Wilson})}, \end{aligned} \quad (97)$$

$$\begin{aligned} O_{v_2,e}^{\overline{\text{MS}}} &= 0.9941 \cdot O_{v_2,e}^{\text{lat}(\text{domain-wall}, M=1.0)} \\ &= 0.97837 \cdot O_{v_2,e}^{\text{lat}(\text{Wilson})}, \end{aligned} \quad (98)$$

$$\begin{aligned} O_{a_2,e}^{\overline{\text{MS}}} &= 0.9941 \cdot O_{a_2,e}^{\text{lat}(\text{domain-wall}, M=1.0)} \\ &= 0.97837 \cdot O_{a_2,e}^{\text{lat}(\text{Wilson})} \end{aligned} \quad (99)$$

$$O_{d_1}^{\overline{\text{MS}}} = 0.9984 \cdot O_{d_1}^{\text{lat}(\text{domain-wall}, M=1.0)}, \quad (100)$$

$$\begin{aligned} O_{t_1}^{\overline{\text{MS}}} &= 0.8694 \cdot O_{t_1}^{\text{lat}(\text{domain-wall}, M=1.0)} \\ &= 0.85631 \cdot O_{t_1}^{\text{lat}(\text{Wilson})}, \end{aligned} \quad (101)$$

$$\begin{aligned} O_{t_2}^{\overline{\text{MS}}} &= 1.0000 \cdot O_{t_2}^{\text{lat}(\text{domain-wall}, M=1.0)} \\ &= 0.99559 \cdot O_{t_2}^{\text{lat}(\text{Wilson})}, \end{aligned} \quad (102)$$

where for comparison the corresponding Wilson results are also shown. Of course the domain-wall renormalization factors vary with  $M$ . For example, for  $M = 1.8$  (which is almost at the edge of the allowed parameter space) their values are instead

$$O_{v_2,d}^{\overline{\text{MS}}} = 0.9911 \cdot O_{v_2,d}^{\text{lat}(\text{domain-wall}, M=1.8)}, \quad (103)$$

$$O_{a_2,d}^{\overline{\text{MS}}} = 0.9911 \cdot O_{a_2,d}^{\text{lat}(\text{domain-wall}, M=1.8)}, \quad (104)$$

$$O_{v_2,e}^{\overline{\text{MS}}} = 0.9819 \cdot O_{v_2,e}^{\text{lat}(\text{domain-wall}, M=1.8)}, \quad (105)$$

$$O_{a_2,e}^{\overline{\text{MS}}} = 0.9819 \cdot O_{a_2,e}^{\text{lat}(\text{domain-wall}, M=1.8)}, \quad (106)$$

$$O_{d_1}^{\overline{\text{MS}}} = 1.1086 \cdot O_{d_1}^{\text{lat}(\text{domain-wall}, M=1.8)}, \quad (107)$$

$$O_{t_1}^{\overline{\text{MS}}} = 0.8813 \cdot O_{t_1}^{\text{lat}(\text{domain-wall}, M=1.8)}, \quad (108)$$

$$O_{t_2}^{\overline{\text{MS}}} = 0.9942 \cdot O_{t_2}^{\text{lat}(\text{domain-wall}, M=1.8)}. \quad (109)$$

Results for other choices of  $M$  and  $g_0$  can be easily obtained from the numbers presented in this section. Table II contains the values of the renormalization factors as a function of  $M$  for  $g_0 = 1$ .

All the renormalization constants presented in this work can also be used in unquenched simulations, provided that one computes only matrix elements of flavor nonsinglet quark operators, for which at one-loop internal quark loops never appear. The numbers for the transversity operators can be however considered unquenched even in the singlet case, since no chiral-odd gluon operators exist, which would constitute the only possibility for a having a mixing.

We can easily notice that the renormalization corrections that we have obtained for domain-wall fermions are in general small. In particular when the Dirac mass is  $M = 1$  or not too far from it they are not too different from the corresponding Wilson results. In many cases the total renormalization factors turn out to be quite close to 1, reflecting the fact that the domain-wall one-loop amplitudes have almost the same values as the corresponding

TABLE II. Values of the renormalization factors for the various operators, for domain-wall QCD at  $g_0 = 1$  and  $\mu = 1/a$ . We remind that  $Z_{a_2,d} = Z_{v_2,d}$  and  $Z_{a_2,e} = Z_{v_2,e}$ .

$M$	$Z_{v_2,d}$	$Z_{v_2,e}$	$Z_{d_1}$	$Z_{t_1}$	$Z_{t_2}$
0.1	0.9979	0.9945	0.1931	0.8494	0.9952
0.2	0.9984	0.9948	0.6480	0.8529	0.9963
0.3	0.9988	0.9951	0.7958	0.8557	0.9972
0.4	0.9992	0.9952	0.8683	0.8582	0.9980
0.5	0.9995	0.9953	0.9112	0.8604	0.9986
0.6	0.9997	0.9953	0.9396	0.8624	0.9991
0.7	0.9998	0.9951	0.9600	0.8643	0.9995
0.8	0.9999	0.9949	0.9755	0.8661	0.9998
0.9	0.9998	0.9946	0.9879	0.8678	1.0000
1.0	0.9997	0.9941	0.9984	0.8694	1.0000
1.1	0.9994	0.9935	1.0077	0.8710	1.0000
1.2	0.9990	0.9927	1.0164	0.8725	0.9998
1.3	0.9984	0.9917	1.0250	0.8740	0.9995
1.4	0.9976	0.9905	1.0342	0.8754	0.9990
1.5	0.9966	0.9890	1.0446	0.8768	0.9982
1.6	0.9952	0.9872	1.0578	0.8782	0.9973
1.7	0.9934	0.9849	1.0765	0.8797	0.9959
1.8	0.9911	0.9819	1.1086	0.8813	0.9942
1.9	0.9878	0.9780	1.1900	0.8832	0.9917

$\overline{\text{MS}}$  results. The only exception is the tensor charge, which on the other hand is also the only case which for fermions which break chiral symmetry cannot be renormalized, because of its power-divergent mixing. From this point of view, domain-wall fermions appear to behave quite at variance with overlap fermions, for which the renormalization factors are generally not small, giving in many cases rather large one-loop corrections to the tree-level matrix elements [36,37,41]. The origin of most of these large effects can be traced back to the  $\Sigma_1$  contribution from the half-circle diagram of the self-energy, which for overlap fermions is rather big. On the contrary, for domain-wall fermions  $\Sigma_1$  does not deviate too much from the  $\Sigma_1$  of Wilson fermions. Thus, apart from  $O_{d_1}$  when  $M$  is away from one, the renormalization factors computed in this work give small corrections at the standard accessible couplings.

We have computed the bilinears and the self-energy anew, and we have found some discrepancies when comparing our results, which we report in the appendix, with the numbers given in [18]. These discrepancies derive only from the continuum integrals that are needed to compute the divergent terms with the Kawai method (for  $\Sigma_3$  and the tensor charge, which are finite, we completely agree). The differences between our results for the  $R^{\text{lat}}$  quantities and those in [18] are indeed in all cases independent of  $M$  and always are an integer or half-integer number. The  $\overline{\text{MS}}$  renormalization factors given in [18] are also different, and for the same amount, from what is found elsewhere in the literature (e.g., [36,37,41]). All these differences

cancel then in the expressions of the renormalization factors, which do not present any discrepancies with [18].

## VI. CONCLUSIONS

In this paper we have presented the computation of the one-loop renormalization factors of a few operators which measure the first nontrivial moment of various structure functions, giving a complete description of the quark momentum and spin at leading twist. We have used domain-wall fermions, and the associated chiral symmetry plays an important role in the structure of the strong radiative corrections.

We have automated the calculations by developing suitable FORM codes. This will make it easier to consider the case of more complicated operators. The renormalization factors that we have found turn out to be in many cases close to 1.

## APPENDIX: SELF-ENERGY AND BILINEARS

We report here the results for the quark self-energy and the bilinear operators, which were first calculated in [18] in Feynman gauge.

Taking into account that the results for the pseudoscalar and axial-vector operators are equal to the ones for the scalar and vector operators, respectively, and that the tensor operator has been reported in the main body of the paper, the one-loop results for the proper diagrams that we need here are:

TABLE III. Values of the domain-wall constants needed for the renormalization of the self-energy and the bilinear operators. We remind that  $V_p^{\alpha=1} = V_S^{\alpha=1}$  and  $V_A^{\alpha=1} = V_V^{\alpha=1}$ , and that  $z_w = -2w_0\Sigma_3/(1 - w_0^2)$ .

$M$	$\Sigma_1^{\alpha=1}$	$\Sigma_3$	$z_w$	$V_S^{\alpha=1}$	$V_V^{\alpha=1}$
0.1	11.6603	51.0482	-483.6145	7.8219	6.3355
0.2	11.5099	50.7450	-225.5333	8.6070	6.3380
0.3	11.3829	50.4885	-138.5959	9.2424	6.3408
0.4	11.2730	50.2664	-94.2495	9.8020	6.3438
0.5	11.1772	50.0726	-66.7635	10.3176	6.3472
0.6	11.0939	49.9038	-47.5274	10.8074	6.3509
0.7	11.0221	49.7582	-32.8076	11.2834	6.3549
0.8	10.9616	49.6352	-20.6813	11.7549	6.3594
0.9	10.9124	49.5351	-10.0071	12.2296	6.3644
1.0	10.8750	49.4588	0.0000	12.7151	6.3699
1.1	10.8504	49.4084	9.9815	13.2189	6.3762
1.2	10.8399	49.3865	20.5777	13.7496	6.3831
1.3	10.8455	49.3972	32.5696	14.3176	6.3910
1.4	10.8699	49.4461	47.0915	14.9360	6.4000
1.5	10.9170	49.5411	66.0549	15.6225	6.4102
1.6	10.9923	49.6935	93.1753	16.4024	6.4219
1.7	11.1041	49.9198	137.0349	17.3150	6.4356
1.8	11.2652	50.2462	223.3164	18.4274	6.4516
1.9	11.4979	50.7176	480.4824	19.8800	6.4706

$$O_S^{\text{proper}} = \bar{g}^2((-4 + \xi) \log a^2 p^2 + V_S^{\alpha=1} - \xi \cdot 5.792\,010) O_S^{\text{tree}}, \quad (\text{A1})$$

$$O_V^{\text{proper}} = \bar{g}^2((-1 + \xi) \log a^2 p^2 + V_V^{\alpha=1} - \xi \cdot 4.792\,010) O_V^{\text{tree}}. \quad (\text{A2})$$

There is no operator tadpole for the bilinears, and adding the self-energy contribution proportional to  $i\not{p}$  [Eq. (76)]

$$\Sigma_1 = \bar{g}^2((1 - \xi) \log a^2 p^2 + \Sigma_1^{\alpha=1} + \xi \cdot 4.792\,010), \quad (\text{A3})$$

we get, for  $M = 1$ ,

$$O_S^{\text{lat}} = (1 - \bar{g}^2(3 \log a^2 p^2 - 23.5901 + \xi)) O_S^{\text{tree}}, \quad (\text{A4})$$

$$O_V^{\text{lat}} = (1 + \bar{g}^2 \cdot 17.2450) O_V^{\text{tree}}. \quad (\text{A5})$$

The one-loop results in the  $\overline{\text{MS}}$  scheme are [36,37,41]:

$$O_S^{\overline{\text{MS}}} = \left(1 + \bar{g}^2 \left(-3 \log \frac{p^2}{\mu^2} + 5 - \xi\right)\right) O_S^{\text{tree}}, \quad (\text{A6})$$

$$O_V^{\overline{\text{MS}}} = O_V^{\text{tree}}, \quad (\text{A7})$$

and thus

$$O_S^{\overline{\text{MS}}} = 0.8430 \cdot O_S^{\text{lat}(\text{domain-wall}, M=1.0)} = 0.890\,64 \cdot O_S^{\text{lat}(\text{Wilson})}, \quad (\text{A8})$$

$$O_P^{\overline{\text{MS}}} = 0.8430 \cdot O_P^{\text{lat}(\text{domain-wall}, M=1.0)} = 0.809\,22 \cdot O_P^{\text{lat}(\text{Wilson})}, \quad (\text{A9})$$

$$O_V^{\overline{\text{MS}}} = 0.8544 \cdot O_V^{\text{lat}(\text{domain-wall}, M=1.0)} = 0.825\,92 \cdot O_V^{\text{lat}(\text{Wilson})}, \quad (\text{A10})$$

$$O_A^{\overline{\text{MS}}} = 0.8544 \cdot O_A^{\text{lat}(\text{domain-wall}, M=1.0)} = 0.866\,63 \cdot O_A^{\text{lat}(\text{Wilson})}, \quad (\text{A11})$$

where for comparison the corresponding Wilson results are also shown. The renormalization factors for other values of  $M$  and  $g_0$  can be easily obtained from the numbers given in Table III, where we in addition to  $\Sigma_1$  we report also the results for the quantities  $\Sigma_3$  and

$$z_w = -\frac{2w_0}{1-w_0^2} \Sigma_3, \quad (\text{A12})$$

which determines the amount of additive renormalization to  $w_0 = 1 - M$ .

## ACKNOWLEDGMENTS

I am grateful for the support by Fonds zur Förderung der Wissenschaftlichen Forschung in Österreich (FWF), Project No. P16310-N08.

- 
- [1] D. B. Kaplan, Phys. Lett. B **288**, 342 (1992).
  - [2] Y. Shamir, Nucl. Phys. **B406**, 90 (1993).
  - [3] V. Furman and Y. Shamir, Nucl. Phys. **B439**, 54 (1995).
  - [4] P. H. Ginsparg and K. G. Wilson, Phys. Rev. D **25**, 2649 (1982).
  - [5] M. Lüscher, Phys. Lett. B **428**, 342 (1998).
  - [6] Y. Kikukawa, Phys. Rev. D **65**, 074504 (2002).
  - [7] Y. Aoki *et al.*, hep-lat/0508011.
  - [8] C. Dawson, T. Izubuchi, T. Kaneko, S. Sasaki, and A. Soni, hep-lat/0510018.
  - [9] R. G. Edwards, B. Joo, A. D. Kennedy, K. Orginos, and U. Wenger, hep-lat/0510086.
  - [10] K. Hashimoto, T. Izubuchi, and J. Noaki (RBC-UKQCD Collaborations), hep-lat/0510079.
  - [11] H. Lin, S. Ohta, and N. Yamada (RBC Collaboration), hep-lat/0510071.
  - [12] J. Noaki, hep-lat/0510019.
  - [13] N. Yamada, T. Blum, M. Hayakawa, and T. Izubuchi (RBC Collaboration), hep-lat/0509124.
  - [14] B. Bistrovic *et al.* (LHPC Collaboration), hep-lat/0509101.
  - [15] R. G. Edwards *et al.* (LHPC Collaboration), hep-lat/0509185.
  - [16] R. G. Edwards *et al.* (LHPC Collaboration), hep-lat/0510062.
  - [17] K. Orginos, T. Blum, and S. Ohta, hep-lat/0505024.
  - [18] S. Aoki, T. Izubuchi, Y. Kuramashi, and Y. Taniguchi, Phys. Rev. D **59**, 094505 (1999).
  - [19] R. Narayanan and H. Neuberger, Phys. Lett. B **302**, 62 (1993).
  - [20] S. Aoki and H. Hirose, Phys. Rev. D **49**, 2604 (1994).
  - [21] S. Aoki and H. Hirose, Phys. Rev. D **54**, 3471 (1996).
  - [22] P. M. Vranas, Phys. Rev. D **57**, 1415 (1998).
  - [23] Y. Kikukawa, H. Neuberger, and A. Yamada, Nucl. Phys. **B526**, 572 (1998).
  - [24] S. Aoki and Y. Taniguchi, Phys. Rev. D **59**, 054510 (1999).
  - [25] T. Blum, A. Soni, and M. Wingate, Phys. Rev. D **60**, 114507 (1999).
  - [26] S. Aoki and Y. Taniguchi, Phys. Rev. D **59**, 094506 (1999).
  - [27] S. Aoki, T. Izubuchi, Y. Kuramashi, and Y. Taniguchi, Phys. Rev. D **60**, 114504 (1999).
  - [28] J. Noaki and Y. Taniguchi, Phys. Rev. D **61**, 054505 (2000).
  - [29] S. Aoki and Y. Kuramashi, Phys. Rev. D **63**, 054504 (2001).

- [30] S. Aoki, T. Izubuchi, Y. Kuramashi, and Y. Taniguchi, Phys. Rev. D **67**, 094502 (2003).
- [31] S. Aoki and Y. Kuramashi, Phys. Rev. D **68**, 034507 (2003).
- [32] N. Yamada, S. Aoki, and Y. Kuramashi, Nucl. Phys. **B713**, 407 (2005).
- [33] Y. Shamir, Phys. Rev. D **62**, 054513 (2000).
- [34] G. Martinelli and Y.C. Zhang, Phys. Lett. B **123**, 433 (1983).
- [35] S. Capitani, Phys. Rep. **382**, 113 (2003).
- [36] S. Capitani, Nucl. Phys. **B592**, 183 (2001).
- [37] S. Capitani, Nucl. Phys. **B597**, 313 (2001).
- [38] J. A. M. Vermaseren, math-ph/0010025.
- [39] M. Lüscher and P. Weisz, Nucl. Phys. **B266**, 309 (1986).
- [40] H. Kawai, R. Nakayama, and K. Seo, Nucl. Phys. **B189**, 40 (1981).
- [41] C. Alexandrou, E. Follana, H. Panagopoulos, and E. Vicari, Nucl. Phys. **B580**, 394 (2000).
- [42] R. Horsley, H. Perlt, P.E.L. Rakow, G. Schierholz, and A. Schiller (QCDSF Collaboration), Nucl. Phys. **B693**, 3 (2004); **B713**, 601E (2005).